Retrieval of Cloud Properties for Partly Cloudy Imager Pixels

JAMES A. COAKLEY JR., MICHAEL A. FRIEDMAN,* AND WILLIAM R. TAHNK

College of Oceanic and Atmospheric Sciences, Oregon State University, Corvallis, Oregon

(Manuscript received 22 January 2004, in final form 8 July 2004)

ABSTRACT

Retrievals of cloud properties from satellite imagery often invoke the assumption that the fields of view are overcast when cloud-contaminated, even though a significant fraction are only partially cloud-covered. The overcast assumption leads to biases in the retrieved cloud properties: cloud amounts and droplet effective radii are typically overestimated, while visible optical depths, cloud altitudes, cloud liquid water amounts, and column droplet number concentrations are typically underestimated. In order to estimate these biases, a retrieval scheme was developed to obtain the properties of clouds for partially covered imager fields of view. The partly cloudy pixel retrieval scheme is applicable to single-layered cloud systems and invokes the assumption that clouds that only partially cover a field of view are at the same altitude as nearby clouds from the same layer that completely cover imager pixels. The properties of the retrieval are illustrated through its application to 2-km Visible and Infrared Scanner (VIRS) data from the Tropical Rainfall Measuring Mission (TRMM) for a marine stratocumulus scene. The scene was chosen because the cloud properties are typical of such systems based on an analysis of VIRS data for February and March 1998. Comparisons of properties for clouds in partly cloudy pixels and those for clouds in nearby overcast pixels reveal that the optical depths and droplet effective radii are generally smaller for the clouds in the partly cloudy pixels. In addition, for pixel-scale cloud fractions between 0.2 and 0.8, optical depth, droplet effective radius, and column droplet number concentration decrease slowly with decreasing cloud cover fraction. The changes are only about 20%–30%, while cloud cover fraction changes by 80%. For comparison, changes in optical depth and column number concentration retrieved using a threshold method decrease by 80%–90%. As long as the cloud cover in partly cloudy pixels is greater than about 0.1, uncertainties in the estimates of the cloud altitudes and of the radiances for the cloud-free portions of the fields of view give rise to uncertainties in the retrieved cloud properties that are comparable to the uncertainties in the properties retrieved for overcast pixels.

1. Introduction

Current methods for retrieving cloud properties from satellite imagery data commonly take a field of view to be overcast if it is found to have significant cloud contamination. Otherwise, the field of view is taken to be cloud-free. At the 2-km scale examined in this study, the majority of the fields of view are either cloud-free or overcast, and thus satisfy this approximation. Nonetheless, a substantial fraction (~40%) contains broken clouds. The fraction of pixels that are partly cloudy becomes larger at the spatial resolution of imagers used to estimate global cloud properties, such as the 4-km-resolution Global Area Coverage (GAC) data of the Advanced Very High Resolution Radiometer (AVHRR) (Nakajima et al. 2001) and at the 6–8-km resolution of the geostationary imagery used in the International Satellite Cloud Climatology Project (ISCCP; Rossow and Schiffer 1999), but somewhat smaller at the 1-km resolution of the Moderate Resolution Imaging Spectroradiometer (MODIS) (King et al. 2003). Based on evidence presented in section 3, the change in the frequency of partly cloudy pixels is likely to be slight in going from a spatial resolution of 1 to 8 km.

Estimates of cloud properties, such as cloud amount, visible optical depth, droplet effective radius, cloud altitude, etc., retrieved assuming that the fields of view are overcast, when in fact they are only partially covered, will be biased. Numerical simulations of the retrieval process indicate that when clouds become broken and fill only a portion of the field of view, the overcast assumption leads to optical depths that are smaller than the actual values and droplet radii that are larger (Han et al. 1994). Nakajima and Nakajima (1995, their Fig. 17) show retrievals for 4-km AVHRR GAC data in which some of the clouds have relatively small optical depths but relatively large droplet radii. These retrievals suggest that the clouds have unrealistically

*Current affiliation: American Meteorological Society, Boston, Massachusetts.

Corresponding author address: J. A. Coakley Jr., College of Oceanic and Atmospheric Sciences, COAS Admin. 104, Oregon State University, Corvallis, OR 97331-5503.
E-mail: coakley@coas.oregonstate.edu

low column droplet numbers. Some have sought to avoid such retrievals by using the spatial uniformity of emitted radiation for contiguous arrays of pixels to identify imager pixels that are overcast by layered clouds (Wetzel and Stowe 1999; Nakajima et al. 2001; Szczodrak et al. 2001; Harshvardhan et al. 2002). In the case of 1-km MODIS observations, the co-occurrence of large droplet radius and small optical depth in some pixels has been recognized as being due to partial cloud cover within the pixels, and the quality assurance flags for such retrievals have been set to low confidence (Platnick et al. 2003). In addition to the biases in cloud properties, since the anisotropy of the radiances are nonlinearly related to optical depth and, to a lesser extent, droplet radius, the radiative fluxes derived from the biased cloud properties will likewise be biased (Kobayashi 1993).

In order to estimate the possible biases, a retrieval scheme has been developed for obtaining the properties of clouds that only partially cover an imager field of view. The scheme is essentially that proposed by Arking and Childs (1985) but never fully investigated. The scheme is restricted to regions that contain single-layered cloud systems. In such regions, clouds that fail to completely cover an imager's field of view are taken to be part of the same layer, and thus at the same altitude, as nearby clouds that completely fill the field of view. When allowance is made for the partial cloud cover within imager pixels, the average optical depths and droplet effective radii for clouds in pixels that are only partially cloud covered are smaller than those of nearby clouds that completely cover the imager pixels. These characteristics seem plausible as layered clouds appear to thin and droplets appear to evaporate as the layer breaks up. Interestingly, the optical depths, droplet radii, and column droplet number concentrations for the clouds in the partly cloudy pixels depend only weakly on fractional cloud cover, suggesting that these properties remain relatively constant as cloud layers break up.

Here the retrieval scheme is briefly described and the application of the retrieval to a case representative of a single-layered marine stratocumulus system is presented. This example is used to illustrate the differences in the properties of clouds that occupy pixels that are only partially covered and those of nearby clouds that completely cover the imager pixels. The cloud properties retrieved for the partly cloudy pixels are also compared with those derived using the overcast assumption to illustrate some of the biases that arise from threshold retrievals. While the results are presented for only one case, the case was chosen to be representative of retrievals obtained through the analysis of global data. Results of a global analysis will be presented elsewhere. Finally, the results of a sensitivity study are presented to illustrate the uncertainties in the cloud properties retrieved for the partly cloudy pixels based on realistic uncertainties in the knowledge of the layer altitude and the radiances associated with the cloud-free portions of the partly cloudy pixels. As expected, uncertainties in the retrieved cloud properties become sizable as the effect of the clouds on the observed radiances become small: when the clouds are thin, the fractional cloud cover in the pixel is small, and the layer is near the surface. Nevertheless, under most conditions, errors in the properties of the partly cloudy pixels are not unlike those expected for the properties of overcast pixels (Nakajima and King 1990; Han et al. 1994), provided the fractional cloud cover is greater than about 0.1.

2. Method

The partly cloudy pixel retrieval scheme follows an approach proposed by Arking and Childs (1985). Here, the retrieval scheme is applied to the Visible and Infrared Scanner (VIRS) data collected during the Tropical Rain Measuring Mission (TRMM). VIRS is a scanning radiometer with five spectral channels nominally centered at 0.64, 1.6, 3.7, 11, and 12 μm. It has a swath of 261 pixels, a nadir resolution of 2 km, and a maximum scan angle of 45°. The retrievals are performed for orbital segments containing 520 scan lines of the VIRS imagery data. An orbital segment covers approximately 720 km $\times$ 1100 km. Data from VIRS covered the Tropics, nominally 35°S–35°N. Global data for February and March 1998 have been analyzed using the partly cloudy pixel retrieval scheme, but for illustrative purposes, only results for an extensive layer of marine stratocumulus in a single orbital segment are presented.

Partly cloudy pixel retrievals include the following:

1) Scene identification is performed, in which pixels are identified as being either (a) cloud-free, (b) partly cloudy or overcast by clouds that are distributed in altitude, or (c) overcast by clouds in a well-defined layer.
2) A climatology of cloud-free radiances for the period and geographical region of interest is constructed. Cloud-free radiances are used to retrieve the properties of clouds in both overcast and partly cloudy pixels.
3) For each orbital segment an analysis of pixels identified as cloud-free is performed to deduce the radiative properties of the cloud-free background for all locations within the segment. If sufficient numbers of cloud-free pixels are unavailable for estimates of the cloud-free radiances throughout the orbital segment, then the missing cloud-free radiances are drawn from the climatology.
4) Once the cloud-free radiances are determined, cloud properties are retrieved for those pixels found to be overcast by layered cloud systems.
5) The altitudes of the layers derived from the overcast pixels are then analyzed to establish layer altitudes within mesoscale-sized subregions (~50 km) of the orbital segment.

6) Cloud properties are then retrieved for the pixels found to be partly cloudy within the mesoscale-sized subregions for which a layer altitude has been determined.

Specific features of the retrieval steps are described below.

a. Scene identification

The spatial and spectral structure of the radiance fields are used to identify each pixel as being either 1) cloud-free, 2) overcast by optically thick clouds drawn from a layer with a well-defined altitude, 3) partly cloudy, or 4) partly cloudy or overcast by clouds distributed in altitude. The pixel identification scheme is a modified version of the schemes described in Coakley and Walsh (2002) and Coakley et al. (2002). For the scene identification, orbital segments are divided into subregions that are typically 300 km on a side. The results of the identifications are saved for the central portion, typically 250 km on a side, of the subregions. The subregions are overlapped so that, ultimately, all pixels within an orbital segment are identified.

The scene identification is a standalone scheme that was designed to work for ocean regions. First, land areas are identified through pixel-scale reflectances at 0.64 μm, $R_{0.64}$, and 1.6 μm, $R_{1.6}$. A pixel is taken to be mostly land if $R_{1.6}/R_{0.64} > 1.4$. This value was derived empirically and relies on the near-infrared reflectances of vegetation being greater than the visible reflectances. Second, pixels are identified as candidate cloud-free ocean pixels if they lie within a 3×3 pixel array of the 2-km VIRS pixels for which the standard deviation of the 0.64-μm reflectance is less than 0.003 and that for the 11-μm emission is less than 0.5 mW m^{-2} sr^{-1} cm, equivalent to a standard deviation of 0.3 K in the 11-μm brightness temperature for pixels exhibiting emission typical of cloud-free ocean regions. As described by Coakley and Walsh (2002) and Coakley et al. (2002), of the candidate pixels, those identified as being cloud-free ocean are those that pass 0.64-μm reflectance and 11-μm radiance threshold tests. For ocean regions not affected by sun glint, the maximum 0.64-μm reflectance threshold is set at the 90th percentile of the distribution of reflectances obtained for the candidate cloud-free pixels and the minimum 11-μm emission is set at the 10th percentile of the distribution of emitted radiances. Pixels not affected by sun glint are those for which the angle of reflection departs from that for specular reflection from a flat surface by more than 30°.

Once cloud-free pixels have been identified, candidates for pixels overcast by optically thick clouds in a layer with a well-defined altitude are taken to be those that belong to 3×3 pixel arrays that are not cloud-free but exhibit the requisite spatially uniform emission at 11 μm and for which the mean reflectance at 0.64 μm is greater than the 50th percentile of the reflectances for pixel arrays that lack the requisite spatial uniformity in both the reflected and emitted radiances. Pixels that lack spatially uniform emission and reflectances are taken to be partly cloud covered. Again, as described in Coakley and Walsh (2002), overcast pixels are identified as those that pass minimum 0.64-μm reflectance and maximum 11-μm radiance threshold tests and belong to a pixel array that exhibits the requisite spatially uniform emission. The 0.64-μm threshold is taken to be the 5th percentile of the distribution of reflectances found for candidate overcast pixels, and the 11-μm threshold is taken to be the 90th percentile of the 11-μm emission for the candidate overcast pixels.

b. Analysis and climatology of cloud-free radiances

After the cloud-free pixels are identified, a "climatology" is constructed for the angular dependence of the cloud-free 0.64-μm reflectances and 3.7- and 11-μm radiances for the geographic region and time period of interest. This climatology supplies cloud-free radiances for orbital segments that lack sufficient cloud-free pixels to provide estimates of these radiances. For overcast pixels, cloud-free radiances are used to estimate the surface reflectance and the emission incident on the cloud from the surface and the atmosphere beneath the cloud. For partly cloudy pixels, the cloud-free radiances are also assumed to represent the radiances for the cloud-free portion of the pixel.

For the cloud-free climatology, daily means and standard deviations of the cloud-free radiances, and the number of days on which cloud-free radiances were observed, were collected in $2° \times 2°$ latitude–longitude regions for February and March 1998. For each latitude–longitude region, the statistics were binned for satellite zenith angle, in the case of the 11-μm emission, and solar zenith, satellite zenith, and relative azimuth angle for 0.64-μm reflectances and 3.7-μm radiances. Ten-degree bins were used for solar and satellite zenith angles and 20° bins were used for relative azimuth angles. The cloud-free radiances were accumulated separately for each month.

For a particular orbital segment undergoing analysis, once scene identification is performed, pixels found to be cloud-free are used to obtain estimates of the cloud-free radiances for all locations in the orbital segment. For each 50-km-scale subregion (26×26 array of the VIRS 2-km pixels), the 0.64-μm reflectances and 3.7- and 11-μm radiances for the pixels found to be cloud-free are averaged. If at least 5% of the pixels in a subregion are cloud-free, then the average of the cloud-free radiances is used in two-dimensional cubic spline fits, along the orbital track and perpendicular to the orbital track, to obtain cloud-free radiances at the 50-km scale for all portions of the orbital segment. The spline fits are used to interpolate and extrapolate estimates of the cloud-free radiances to 50-km subregions that lack sufficient numbers of cloud-free pixels. Interpolation is allowed for any number of subregions lacking cloud-free pixels that lie between subregions that

contain cloud-free pixels. Extrapolation extends estimates of the cloud-free radiances only to subregions that are adjacent to and lie on the perimeter of subregions that have cloud-free pixels. If interpolation and extrapolation fail to populate all 50-km subregions of the orbital segment with estimates of the cloud-free radiances, then the cloud-free climatology is used to fill in the missing estimates.

c. Retrieval of properties for pixels found to be overcast and analysis of layer altitudes

Once the properties of the cloud-free background have been determined, retrievals are performed for the fields of view found to be overcast by optically thick clouds that are part of a layer with a well-defined altitude, as deduced from the scene identification. The overcast pixel retrieval scheme is a modified version of the scheme used in Coakley and Walsh (2002) and follows the procedures described by Han et al. (1994). The retrievals produce visible optical depths, droplet effective radii, and cloud layer altitudes for the overcast pixels. Layer altitudes for the overcast fields of view are deduced from the surface temperature, the cloud emission temperature, and analyzed meteorological fields for the temperature and water vapor profiles used to calculate the lookup table of emitted radiances. For this study, climatological tropical mean profiles of temperature and humidity have been used in the retrievals (McClatchey et al. 1972).

As was done with the radiances for the cloud-free pixels, the cloud altitudes derived from the overcast fields of view are analyzed on the 50-km scale to determine layer altitudes for adjacent 50-km-scale regions that contain clouds but in which the clouds fail to completely cover at least 5% of the pixels. For the cloud layer altitudes, as opposed to the cloud-free radiances, interpolation and extrapolation are arbitrarily limited to subregions that are adjacent to other subregions that have sufficient numbers of overcast pixels. For cloud-free radiances, interpolation might be extended over several 50-km-scale regions as long as the region missing cloud-free pixels is surrounded by subregions that have sufficient numbers. The arbitrary limitation in the case of layer altitudes is imposed because reliable methods for estimating layer altitudes at arbitrary distances from pixels found to be overcast await development.

In addition, for the purpose of analyzing layer altitudes, each subregion is assumed to contain only one layer. In the current scheme, two-dimensional spline fits are used to map the pixel-weighted average layer altitudes over the domain of qualifying subregions. When more than one layer is present, the layer altitude becomes the pixel-weighted average altitude of the layers. Multilayered cloud systems are fairly common for 50-km-scale regions of the ocean. Use of an average layer altitude in partly cloudy pixel retrievals in cases when multiple layers are present will lead to errors in the retrieved cloud properties. Clearly, an improvement over the current approach would be to use a simple clustering scheme, like that described by Coakley and Baldwin (1984), to identify distinct layers within an orbital segment and then analyze the altitude of each layer separately.

d. Retrievals for partly cloudy pixels

With the retrievals for the overcast pixels performed and layer altitudes determined at the 50-km scale, retrievals of the properties for partly cloudy pixels are performed. Retrievals for partly cloudy pixels are performed only within subregions that are found to have a cloud layer. As described in the previous section, a subregion is identified as having a cloud layer if it either has a sufficient number of overcast pixels or it is adjacent to one or more subregions that have sufficient numbers of overcast pixels. The altitude of the clouds in the partly cloudy pixels is set equal to the altitude analyzed for the cloud layer within the subregion. When the subregion contains only a single cloud layer, the altitudes of the clouds in the partly cloudy pixels are likely to be close to the analyzed altitude. In subregions that contain multiple layers, the analyzed altitude is close to the pixel-weighted average of the altitudes for the pixels found to be overcast within the subregion or in the neighboring subregions. In these subregions, the analyzed altitude is unlikely to be representative of the altitudes of the clouds in the partly cloudy pixels and, consequently, the retrieved properties will be in error. For February and March 1998, approximately 70% of all 50-km-scale oceanic regions were either cloud-free or contained low-level (altitude < 4 km) clouds. Of this 70%, approximately 40%, or 30% of all 50-km-scale oceanic regions, were successfully analyzed using the procedures described here. The regions containing low-level clouds that could not be analyzed had sparse cloud cover. They lacked sufficient numbers of overcast pixels, either within themselves or in surrounding regions, to permit an analysis of layer altitude.

For 50-km subregions in which a cloud layer altitude has been derived, the radiances for the partially covered pixels are assumed to be given by

$$I = (1 - A_C)I_S + A_C I_C(\tau, R_e, z_C), \tag{1}$$

where A_C is the fractional cloud cover for the pixel, I_S is the average radiance associated with the cloud-free portion of the pixel, and $I_C(\tau,R_e,z_C)$ is the average radiance associated with the portion of the pixel that is overcast. For the analyzed altitude, z_C, I_C is a function of the visible optical depth of the clouds, τ, and the droplet effective radius, R_e. The cloud-free radiances used for the partly cloudy pixels are the analyzed radiances described earlier.

For the VIRS observations, the fractional cloud cover, visible optical depth, and droplet effective radius of the clouds in the partly cloudy pixels are adjusted until radiances calculated at 0.64, 3.7, and 11 μm agree

with those observed. The adjustment is iterative. First, the cloud fraction is adjusted until the 11-μm radiance matches the observed radiance. Initially, the cloud is assumed to be opaque ($\tau = 64$) and the effective droplet radius is taken to be $R_e = 6$ μm. If the 11-μm radiance for the partly cloudy pixel, I, is greater than the 11-μm radiance for the cloud-free portion of the pixel, I_S, then the pixel is taken to be cloud-free and no cloud properties are derived for such pixels. Based on the analysis of all VIRS data for February and March 1998, about 4% of all pixels in 50-km-scale regions that contain only low-level, single-layered cloud systems have cloud cover set to zero by the partly cloudy pixel retrieval scheme. For the example reported in the next section the fraction is 3.5%. Understandably, surface temperatures and cloud-free reflectances for the pixels initially identified as cloud-free differed from those initially identified as partly cloudy but which, through the retrieval process, were determined to be cloud-free. For the 50-km-scale subregions that contained both types of pixels, the surface temperatures and 0.64-μm reflectances derived from the pixels initially identified as partly cloudy were on average 0.2 K and 0.003 higher than those derived for the pixels initially identified as cloud-free. Owing to the higher reflectances, these pixels are thought to be cloud-contaminated, but given the similarity in the distribution of emitted and reflected radiances with those obtained for pixels initially identified as cloud-free, the level of contamination is slight. Nevertheless, the contamination precludes the use of such pixels for the determination of such things as aerosol burdens and ocean color that require cloud-free conditions.

Similarly, if the 11-μm radiance for a pixel that is initially identified as partly cloudy is less than the emission expected for opaque clouds that completely cover a pixel, $I_C(\tau = 64, R_e = 6\ \mu\text{m})$, then the pixel is taken to be overcast and the retrieval scheme used for overcast pixels is applied. The altitude of such pixels is recalculated in the overcast pixel retrieval scheme. In the analysis of VIRS data for February and March 1998, for the 50-km-scale regions that contained only low-level, single-layered cloud systems, 17% of the pixels had cloud cover fractions set to unity by the partly cloudy pixel retrieval scheme. For the example described in the next section, the fraction is 16.6%. As with the cloud-free pixels, understandably, the altitudes of the pixels initially identified as overcast differed from those that were initially identified as partly cloudy but which, through the retrieval process, were determined to be overcast. For the 50-km-scale regions that contained both types of pixels, the altitudes of the clouds derived from the pixels initially identified as being partly cloudy were on average 30 m higher than those of the pixels initially identified as being overcast.

For partly cloudy pixels that yield a fractional cloud cover, $0 < A_C < 1$, the visible optical depth is adjusted until the 0.64-μm reflectance calculated for the overcast portion of the pixel matches the observed reflectance, $I_C(\tau,R_e,z_C)$, which is derived from (1) using the current estimate of the fractional cloud cover, A_C. Initially, the droplet effective radius is set at $R_e = 6$ μm. The effective radius is adjusted until the reflectance at 3.7 μm for the overcast portion of the pixel matches the observed reflectance. The 3.7-μm reflectance of the cloud-free ocean background is taken to be zero. Thermal emission is calculated from the sea surface temperature analyzed for the subregion and the atmospheric profiles of temperature and humidity. The emission at 3.7 μm for the overcast portion of the pixel is derived using the layer altitude, the optical depth of the cloud, and the current estimate of the droplet effective radius. The initial value of the droplet effective radius is used in the first iteration. The reflected radiance at 3.7 μm is obtained by subtracting the emitted radiance from the total radiance, reflected plus emitted, calculated for the overcast portion of the pixel from (1).

The above steps are repeated until successive iterations fail to change the cloud fraction, visible optical depth, or droplet effective radius appreciably: $|\Delta A_C| < 0.05$, $|\Delta\tau| < 0.5$, and $|\Delta R_e| < 0.2$ μm. Typically, convergence is achieved on the second iteration. In approximately 5% of all pixels containing clouds that satisfy the conditions for single-layered systems, the retrieval fails. The retrieval fails if the search for the properties that match the observed radiances ranges beyond the domain of the tables of precalculated radiances: $0 \le z_C \le 6$ km, $1 \le \tau \le 64$, and $3 \le R_e \le 42$ μm.

3. Results

The retrieval scheme and the consequences of the retrievals are illustrated through an example. Figure 1 shows an orbital segment (261 scan spots $\times$ 520 scan lines) constructed from 2-km VIRS 0.64- and 11-μm radiances. Most of the orbital segment is covered by low-level marine stratus. Emission at 11 μm reveals upper-level cloud systems in the upper-left corner and near the right edge of the image. The boxed region, which is selected for analysis, contains only low-level marine stratocumulus and covers an area of approximately 290 km by 650 km. It was selected because it contains nearly equal numbers of cloud-free and overcast fields of view as well as a sizeable fraction of partly cloudy fields of view. Of the 2-km VIRS pixels, 26% are cloud-free and 26% are overcast. Based on an analysis of VIRS data for February and March 1998, these frequencies are typical of the global occurrences for 50-km-scale ocean regions that contain single-layered, low-level systems. For such systems, approximately 30% of the 2-km pixels are cloud-free, 30% are overcast, and 40% are partly cloud covered.

Figure 2 shows the pixel-scale fractional cloud cover, cloud visible optical depth, and cloud droplet effective radius retrieved for the boxed region in Fig. 1 using

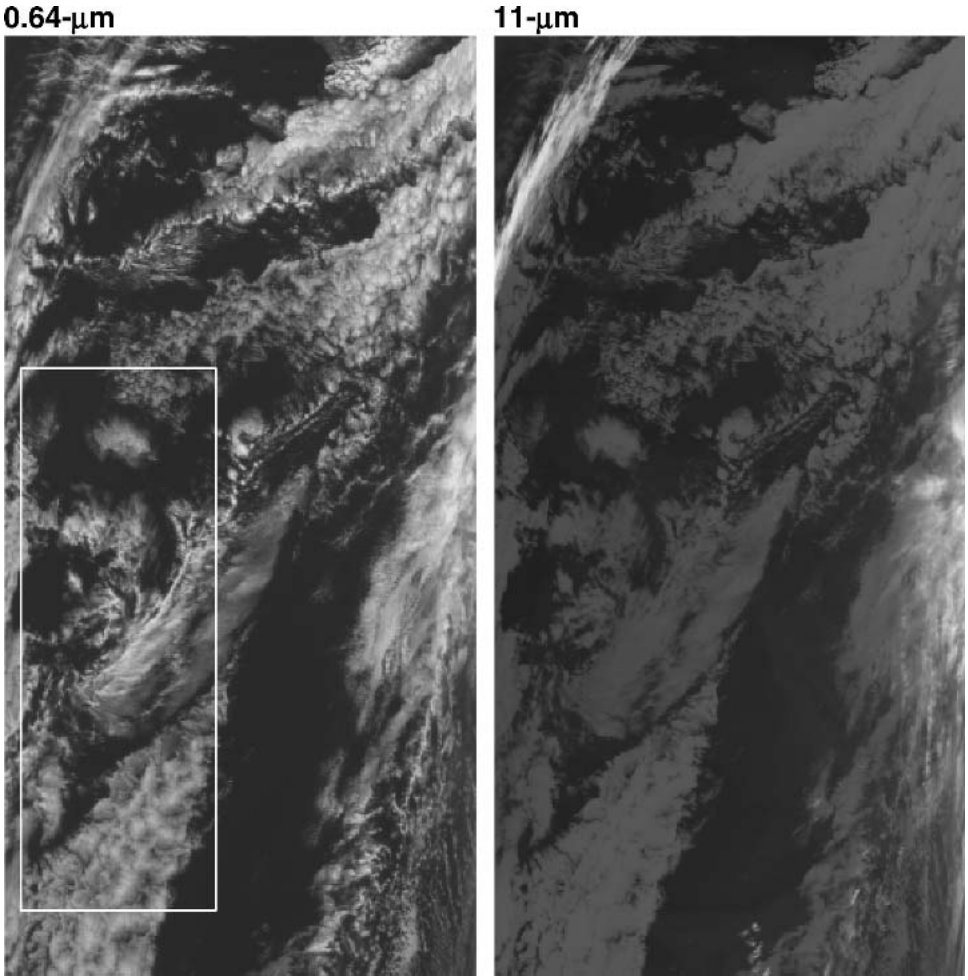

FIG. 1. The 0.64- and 11-μm images derived from 2-km VIRS imagery. The images show a low-level marine stratocumulus system on 1 Feb 1998 off the west coast of Australia at 0102 UTC. This location is near the turning point of the TRMM satellite. The top edge of the image is the easternmost and the left edge is the northernmost portion of the image. The boxed region is chosen for the analyses shown in Figs. 2–11. It was selected because it contained a single-layered cloud system. There is no overlap evident from the upper-level systems in the upper-left corner and central-right edge of the image. The boxed region also contains roughly equal numbers of cloud-free and overcast 2-km fields of view. The region is 108 scan spots $\times$ 300 scan lines and covers approximately 290 km $\times$ 650 km. The center of the boxed region is at 32.5°S, 107.8°E. The solar zenith angle at the center of the boxed region is 56.0°.

both the partly cloudy pixel retrieval scheme and a conventional threshold scheme in which cloud contaminated pixels are taken to be overcast. For the threshold scheme, any partly cloudy pixel found to have a cloud fraction greater than 0.2 is taken to be overcast. The threshold cloud cover fraction for the region is 0.67. For comparison, applying the temperature and visible radiance thresholds prescribed for ISCCP (Rossow and Garder 1993) to the scene produces a cloud cover fraction of 0.64. The fractional cloud cover obtained with the partly cloudy pixel retrieval is 0.57. The threshold retrievals are appropriate for pixels that are overcast and for pixels that are cloud-free. Where pixels are only partially covered, the cloud cover fraction obtained with the threshold is, of course, overestimated, the optical depth is underestimated, and the droplet effective radius is overestimated. This outcome was predicted by Han et al. (1994).

a. Fractional cloud cover

Figure 3 shows the pixel-scale distribution of fractional cloud cover. A feature of the partly cloudy pixel retrieval scheme not shared by threshold schemes is that the regional-scale and even the pixel-scale cloud fraction is relatively insensitive to the spatial resolution of the instrument. In the case shown, VIRS observations were averaged for 3 $\times$ 3 arrays of the 2-km pixels to form 6-km-scale radiances. The averaged radiances were then used to retrieve the cloud properties. As expected, at the 6-km scale, the frequencies of cloud-

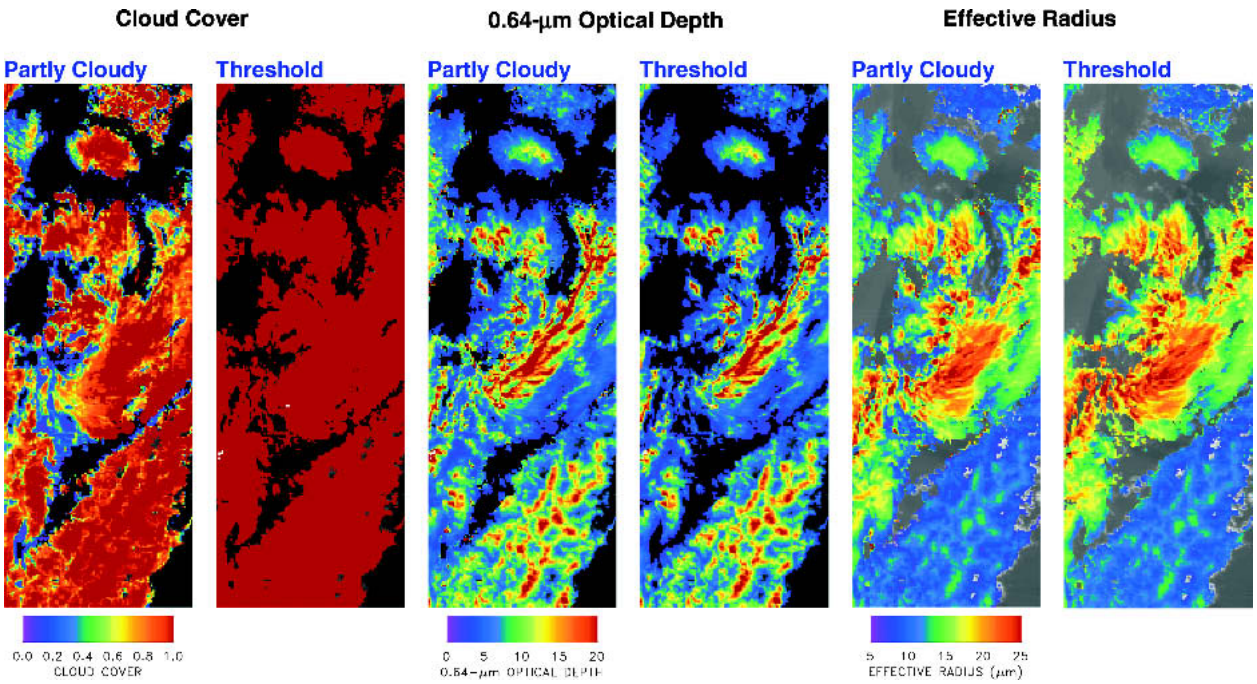

FIG. 2. Pixel-scale cloud fraction, cloud optical depth, and effective droplet radius retrieved while accounting for fractional cloud cover in the 2-km fields of view (partly cloudy) and by applying a threshold retrieval for which the field of view is taken to be overcast if the pixel-scale cloud fraction is greater than 0.2 (threshold). The retrievals are for the boxed region shown in Fig. 1. The retrieved properties are shown overlying the grayscale image of the 0.64-μm reflectances in the case of cloud cover and optical depth and overlying the grayscale image of the 3.7-μm radiance in the case of effective radius. The grayscale portions of each image identify cloud-free pixels.

free and overcast pixels decrease and the frequency of partly cloudy pixels increases, but the changes are slight, suggesting that in going from the 2-km VIRS pixels to the 1-km MODIS pixels, the changes in frequencies will likewise be small. The partly cloudy pixel retrieval scheme gives a cloud fraction of 0.57 for the 2-km observations and 0.58 for the 6-km observations. For the threshold retrievals, the regional cloud cover is 0.67 for the 2-km radiances and 0.72 for the 6-km radiances if the thresholds used in the retrieval scheme are adjusted for the 6-km data. In other words, following rules like those employed to create the ISCCP thresholds, going from an instrument that has a resolution of 2 km to an instrument having a resolution of 6 km will give rise to a modest increase in cloud cover fraction, depending, as discussed below, on the population of partly cloudy pixels at the two spatial scales. If, on the other hand, the threshold results were checked for sensitivity to spatial resolution in the same manner that the partly cloudy pixel retrieval is checked, the thresholds derived for the 2-km data would be applied to 6-km pixels and the resulting cloud cover fraction would be 0.82. Of course, the departure in the threshold results depends on the structure of the clouds within the region (Coakley 1987). If the clouds were distributed so as to create larger percentages of cloud-free and overcast pixels at the 6-km scale, then the departure would decrease; conversely, if the clouds were distributed so as to create smaller percentages of cloud-free and overcast pixels at the 6-km scale, then the departure would increase. At the pixel scale, the partly cloudy pixel retrieval scheme gives cloud fractions for the 6-km pixels that are within an rms difference of 0.09 in cloud cover fraction as derived by averaging the cloud cover fractions obtained for the 2-km retrievals.

b. Optical depth

Figure 4 shows optical depths for overcast and partly cloudy pixels. The figure shows the results of the threshold retrievals (dashed–dotted line) only for those pixels identified as being partly cloud covered by the partly cloudy pixel retrievals. For the pixels identified as overcast, the threshold and the partly cloudy pixel retrievals produce identical properties. For the partly cloudy pixels, assuming that the pixels are overcast, when they are only partially covered, gives rise to optical depths that are smaller than those obtained with the partly cloudy pixel retrieval. Figure 5 shows the optical depths of clouds for pixels having a given fractional cloud cover. Results are shown for both the partly cloudy pixel retrievals (solid curve) and threshold retrievals (dashed line). In the figure the symbols represent the means of the optical depths for the given fractional cloud cover interval and the error bars represent the range of optical depths for pixels with fractional cloud cover falling within 0.05 intervals of the

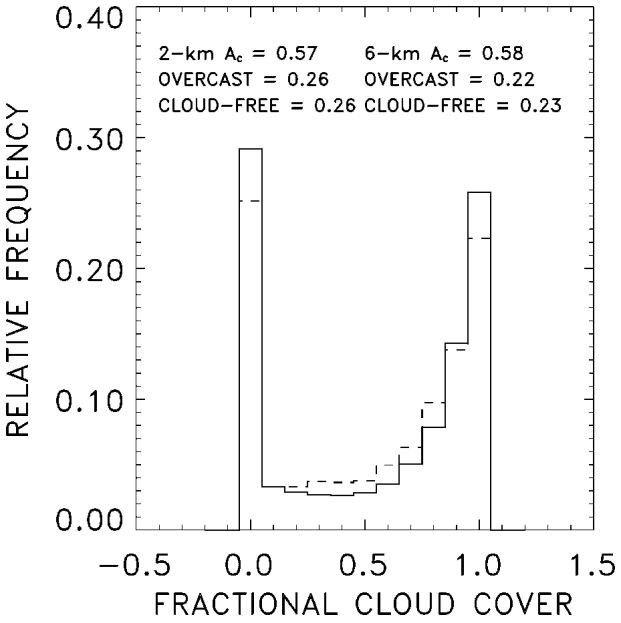

FIG. 3. The 2- (solid line) and 6-km (dashed line) pixel-scale fractional cloud cover for the boxed region shown in Fig. 1. The 6-km pixels were obtained by averaging the radiances for 3×3 arrays of the 2-km pixels.

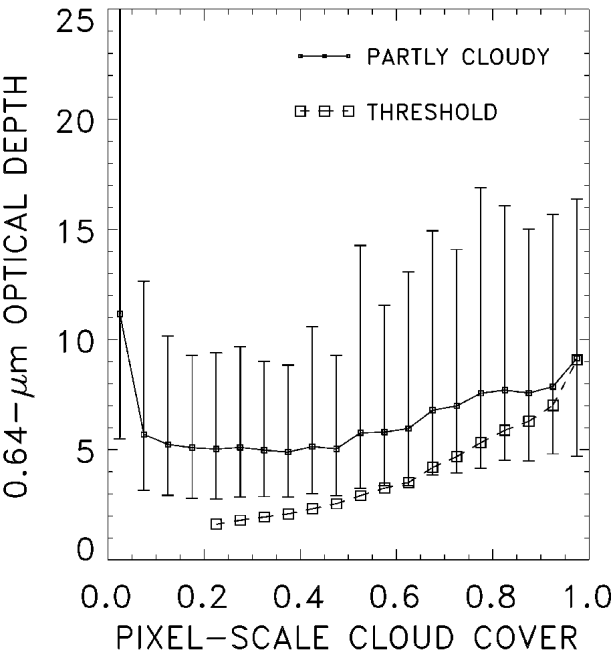

FIG. 5. Pixel-scale cloud optical depth for partly cloudy pixel (solid line) and threshold (dashed line) retrievals as a function of pixel-scale fractional cloud cover obtained with the partly cloudy pixel retrieval. The points give the average of the optical depth for each 0.05 interval in fractional cloud cover. Error bars are given for the partly cloudy pixel retrievals. The error bar below the average value is the root-mean square of the departure of the optical depths from the average value for those that fall below the average within the interval, and that above the average gives the corresponding root-mean-square of the departures that exceed the average value.

fractional cover. The error bars extending downward from the average values depict the root-mean square of the departure of the optical depths from the average for those values that fell below the average. Likewise, the error bars extending upward from the average values depict the corresponding root-mean square of the departures for the optical depths that were above the average value. The error bars are shown only for the partly cloudy pixel retrievals. The ranges obtained with the threshold retrievals are comparable. The figure shows that the optical depths of the clouds in the partly cloudy pixels are relatively insensitive to pixel-scale cloud cover fraction for $0.1 < A_C < 0.5$. The rapid rise in optical depth with cloud fraction for $A_C < 0.1$ is unrealistic. As will be discussed in section 4, uncertainties in the retrieved cloud properties become large as the pixel-scale cloud cover becomes small. For $A_C > 0.5$ the optical depth slowly grows with increasing pixel-scale cloud cover fraction. Part of this growth is undoubtedly due to the thickening of the clouds in regions where cloud cover becomes extensive. The rapid rise in optical depth for $A_C > 0.9$ may also be due to three-dimensional radiative transfer effects. As the separation between the clouds becomes comparable to the cloud thickness, radiation escaping through the sides of clouds has a high probability of being scattered upward by nearby clouds, thereby contributing significantly to the reflected radiances (Welch and Wielicki 1985). In

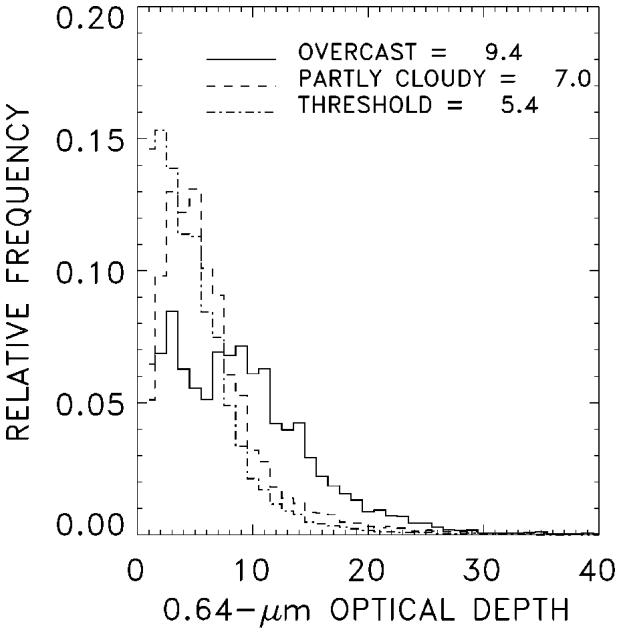

FIG. 4. Cloud optical depth derived for overcast (solid line) and partly cloudy pixels. For the partly cloudy pixels results are presented for both the partly cloudy pixel (dashed line) and threshold (dashed–dotted line) retrievals. Mean values of the optical depths are also given.

any case, for $0.2 < A_C < 0.8$, the optical depth changes little as the fractional cloud cover changes by a factor of 4. Here the relative difference in a cloud property, such as optical depth, is used as a measure of the change for a given change in pixel-scale fractional cloud cover. For optical depth, the relative difference is the difference in the optical depths for the two distinct cloud cover fractions divided by the average of the two optical depths. The relative difference in optical depths between pixels with cloud cover $0.2 < A_C < 0.4$ and those with $0.6 < A_C < 0.8$ is 19%. For threshold retrievals the relative difference is 83%. The relative change in the cloud cover fraction is 80%.

c. Droplet effective radius

Figure 6 shows droplet effective radius for overcast and partly cloudy pixels. Based on the results of the partly cloudy pixel retrievals, the droplet effective radius is smaller for the clouds in the partly cloudy pixels. The threshold retrievals, on the other hand, give a droplet effective radius that is even larger than that obtained for the overcast pixels. The relative magnitudes of the threshold-derived droplet effective radius for the partly cloudy and overcast fields of view depend, of course, on the structure of the clouds within the region. In particular, if the clouds are sufficiently optically thin, then the threshold-derived droplet effective radius will be smaller for the partly cloudy pixels, as is illustrated in Nakajima and Nakajima (1995, their Fig. 17). Figure 7 shows that the droplet effective radius for clouds within partly cloudy pixels decreases with decreasing pixel-scale cloud cover fraction, but the change in droplet size is small. The relative difference in droplet effective radius between pixels with cloud cover $0.2 < A_C < 0.4$ and those with $0.6 < A_C < 0.8$ is 20%. For threshold retrievals the relative difference is only 2%, but the droplet radii for pixels with the smaller cloud cover fractions are larger than those with the larger cloud cover fractions.

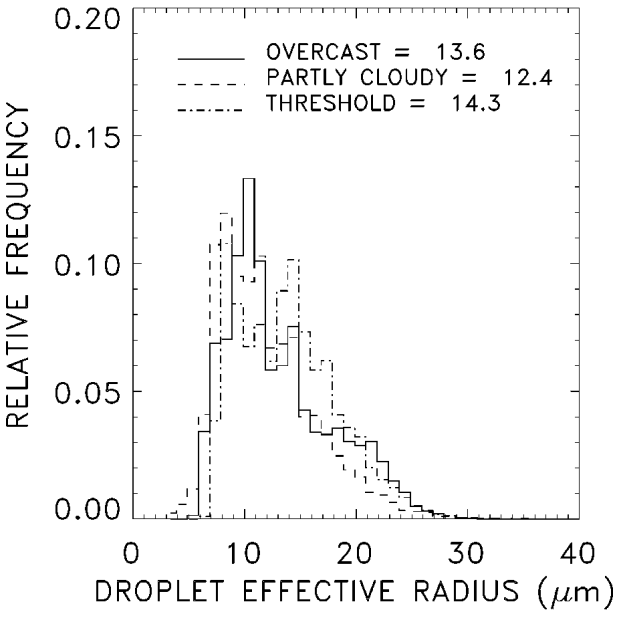

FIG. 6. Same as Fig. 4 but for droplet effective radius.

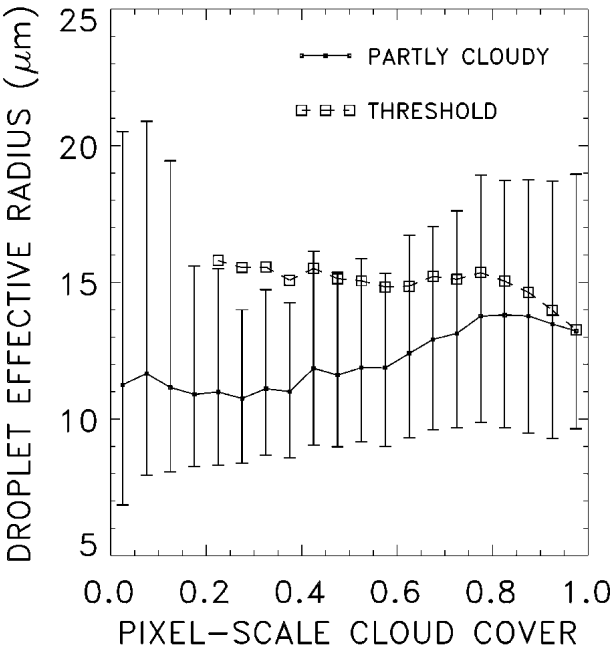

FIG. 7. Same as Fig. 5 but for droplet effective radius.

d. Cloud liquid water path

Figure 8 shows cloud liquid water paths for overcast and partly cloudy pixels. The liquid water path, W, is taken to be given by

$$W = \frac{2}{3}\tau R_e \rho, \tag{2}$$

where $\rho = 1$ g cm^{-3} is the density of water. In the partly cloudy pixels, the threshold-derived optical depths are smaller but the droplet effective radii are larger than those obtained with the partly cloudy pixel retrieval. The net result is that the threshold-derived liquid water path is closer to the value given by the partly cloudy pixel retrieval than is the case for either optical depth or droplet radius. Nevertheless, the threshold-derived liquid water path for the partly cloudy pixels is 10% less than is estimated with the partly cloudy pixel retrieval. Figure 9 shows that the pixel-scale cloud liquid water path, like the optical depth and droplet effective radius, is relatively insensitive to pixel-scale cloud cover fraction for $A_C < 0.5$. The relative difference in liquid water path between pixels with cloud cover $0.2 < A_C < 0.4$ and those with $0.6 < A_C < 0.8$ is 47%. For threshold

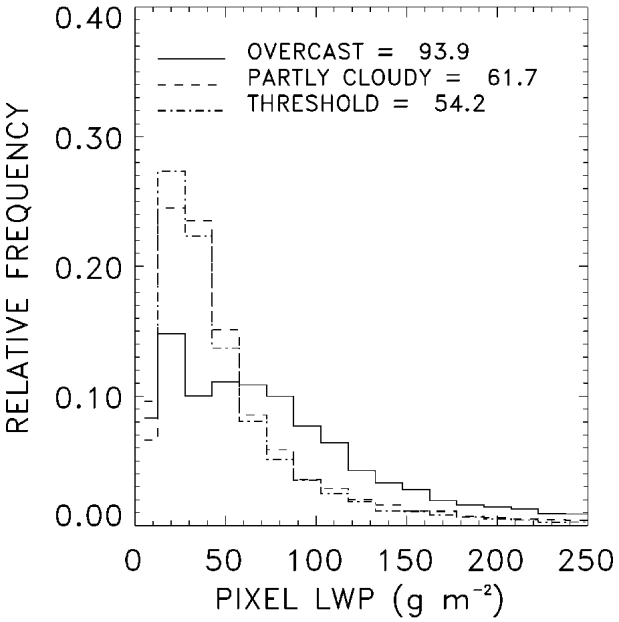

FIG. 8. Same as Fig. 4 but for cloud liquid water path.

retrievals the relative difference is 85%. Owing to the increase of both optical depth and droplet effective radius with cloud cover fraction for $A_C > 0.5$, the liquid water path is more sensitive than either the optical depth or the droplet effective radius to the cloud cover fraction. The range of possible values for the liquid water path, as indicated by the size of the error bars in Fig. 9, also increases as the liquid water path itself increases.

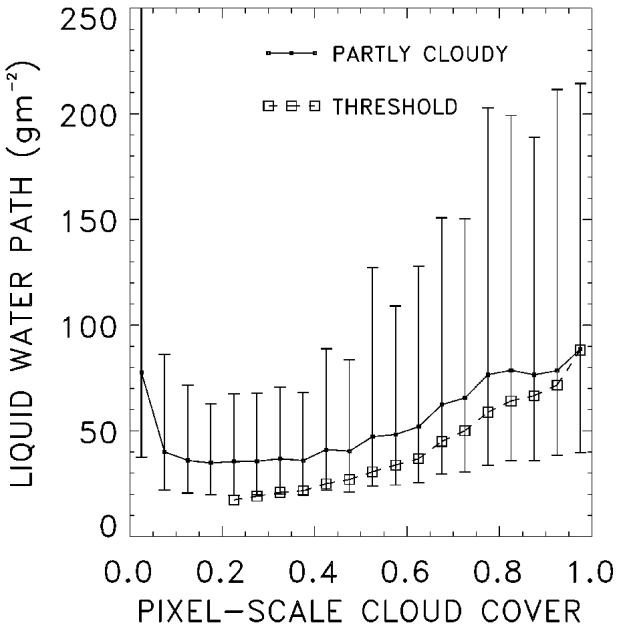

FIG. 9. Same as Fig. 5 but for cloud liquid water path.

e. Column droplet concentration

In models of cloud formation through adiabatic ascent, the volume droplet number concentration remains constant as droplet radius and liquid water concentration increase with altitude above cloud base. The constancy of droplet number concentration with altitude has been found in aircraft observations of low-level marine clouds, and for localized regions, retrievals of the column droplet number concentration for pixels overcast by low-level stratus has been found to be relatively constant (Brenguier et al. 2000; Szczodrak et al. 2001). Figure 10 shows column droplet number concentration and pixel-scale fractional cloud cover. In this study the column number concentration is approximated by

$$nL = \frac{\tau}{2\pi R_e^2}, \tag{3}$$

where n is the volume droplet concentration and L is the thickness of the cloud. As with the optical depths, retrievals of droplet number concentrations become unreliable when the contribution of the overcast portion of the pixel to the observed radiance becomes small, as when cloud cover fractions become small, $A_C < 0.2$. The results show that for pixels with sufficient cloud cover, $A_C > 0.2$, the column droplet number concentration is relatively insensitive to the pixel-scale cloud fraction. The relative difference in column number concentration between pixels with cloud cover $0.2 < A_C < 0.4$ and those with $0.6 < A_C < 0.8$ is 32%, with the number concentration being larger for the pixels

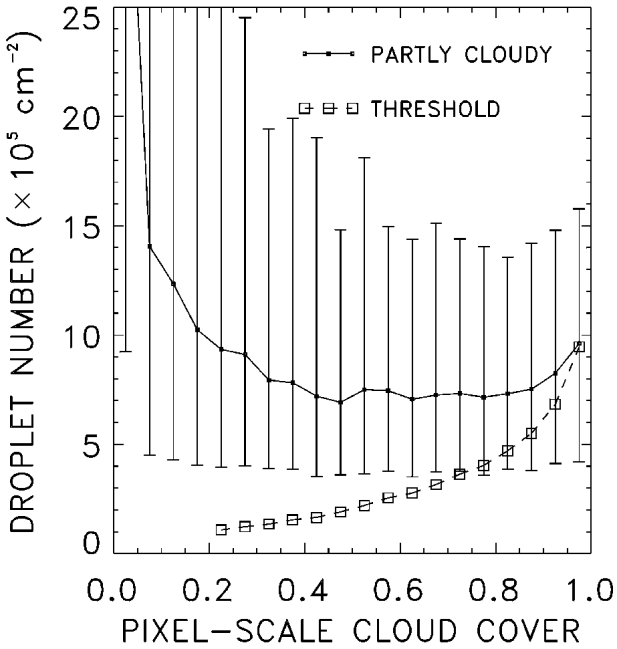

FIG. 10. Same as Fig. 5 but for column droplet number concentration.

with the smaller cloud cover fraction. For threshold retrievals the relative difference is 90%, with the pixels having the greater fractional cloud cover having almost 3 times the number concentration of those with the smaller fractional cloud cover.

While the results shown in Figs. 5, 7, 9, and 10 summarize trends for the entire boxed region in Fig. 1, similar results hold for the 50-km-scale subregions within the box. As low-level marine clouds break up, optical depth, droplet effective radius, and column number concentrations vary little with fractional cloud cover for $0.2 < A_C < 0.8$ within the 2-km pixel scale.

f. Cloud altitude

Figure 11 shows distributions of the cloud altitudes derived using both the partly cloudy pixel and threshold retrievals. Because the altitudes of the partly cloudy pixels are taken to be the same as those of nearby overcast pixels, the altitudes attributed to the partly cloudy pixels in the partly cloudy pixel retrievals are nearly identical to those derived for the overcast pixels. The altitudes for the overcast pixels are slightly higher because the layer altitudes used in the partly cloudy pixel retrievals are derived only from those pixels found to be overcast by the scene identification scheme. As was noted in the previous section, once layer altitudes have been determined for the 50-km subregions within an orbital segment, some of the pixels originally identified as being partly cloudy will be treated as overcast when the 11-μm radiance of the pixel is less than that expected for opaque clouds completely covering the pixel. The altitudes of these clouds are generally greater than the altitude assumed for the partly cloudy pixels within the subregion. The altitudes derived using the threshold method are generally smaller than the layer altitude assumed for the partly cloudy pixel. In the threshold scheme, the pixel is taken to be overcast, even when it is not. Consequently, the large emission from the cloud-free portion of the pixel is taken to be evidence that the cloud is at an altitude below its actual altitude. This behavior is sometimes masked by binning clouds into altitude ranges. In ISCCP, for example, cloud altitude is associated with a pressure level and clouds are placed into three broad ranges of pressure associated with low-, middle-, and upper-level clouds.

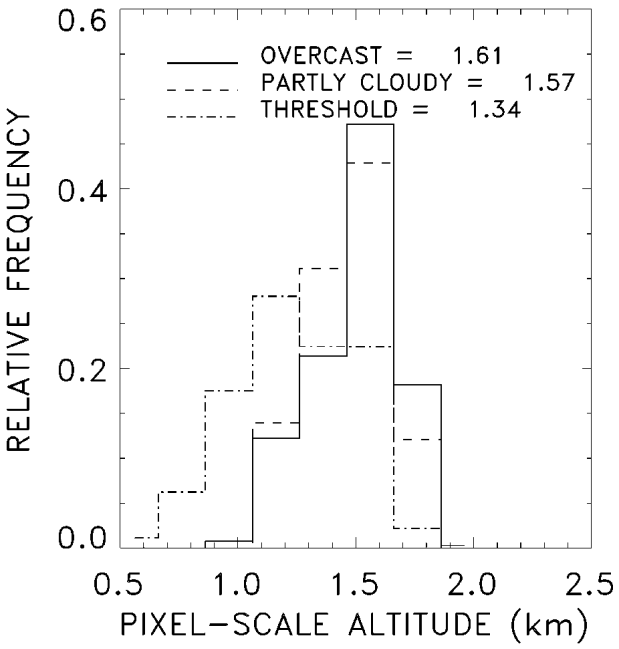

FIG. 11. Same as Fig. 4 but for cloud altitude.

g. Regional averages

Of course, differences between the properties derived using the partly cloudy pixel and threshold retrievals become small when the results for the partly cloudy pixels are averaged with those for the overcast pixels. The regional average cloud optical depth is given by

$$\langle \tau \rangle = \frac{\sum_i A_{Ci}\tau_i}{\sum_i A_{Ci}}, \tag{4}$$

where the sums are over the cloud-contaminated pixels. For the partly cloudy pixel retrievals A_C is the pixel-scale fractional cloud cover. For the threshold retrievals $A_C = 1$. Similar expressions are used to obtain regional estimates of the droplet effective radius, cloud altitude, liquid water path, and column droplet number concentrations. Dividing the boxed region in Fig. 1 into 50-km-scale subregions yields differences between the partly cloudy pixel and threshold retrievals (threshold − partly cloudy) of -1.3 ± 1.2 (mean $\pm$ standard deviation) for cloud optical depth, 0.9 ± 0.7 μm for droplet effective radius, -11 ± 12 g m^{-2} for liquid water path, and $-2.0 \pm 1.3 \times 10^5$ cm^{-2} for the column droplet number concentration. The average cloud properties derived for the partly cloudy pixel retrieval are 7.5 for optical depth, 12.8 μm for droplet effective radius, 71 g m^{-2} for liquid water path, and 8.2×10^5 cm^{-2} for the column droplet number concentration. These results are consistent with the suggestion made by Rossow et al. (2002) that thresholds applied to radiances at the 3–5-km scale should be adequate for determining regional estimates of cloud properties. Nevertheless, biases are clearly detectable, and at these levels, the differences between the partly cloudy pixel and threshold-derived regional average cloud properties, even with the partly cloudy properties weighted by the fractional cloud cover, become appreciable fractions of the region-to-region variability. For the case under study the standard deviations of the average properties for the 50-km-scale subregions are 3.0 for optical depth, 3.3 μm for droplet effective radius, 44 g m^{-2} for liquid water

path, and 4.2×10^5 cm^{-2} for column droplet number concentration.

An advantage of the proposed partly cloudy pixel retrieval scheme is that it facilitates the comparison of cloud properties for clouds in fields of view that are only partially covered with those in nearby fields of view that are overcast. For example, for the region under study, average differences in optical depths, droplet effective radii, cloud liquid water path, and column droplet number concentration between clouds in partly cloudy pixels and those in nearby overcast pixels can be inferred from the results shown in Figs. 4–10. Such information could prove useful in developing cloud models such as, for example, the large eddy simulation model described in Stevens et al. (1998).

4. Sensitivity of cloud properties to uncertainties in cloud altitude and cloud-free radiances

The properties of clouds that only partially cover an imager pixel are subject to uncertainties in the radiances attributed to the cloud-free portion of the pixel and in the altitude taken for the cloud layer. Examples of the sensitivity are shown in Fig. 12. The results in the figure were generated using radiances simulated for a partly cloudy pixel. The clouds in the pixel were given a visible optical depth, $\tau = 7.5$, and an effective radius, $R_e = 12.8$ μm, the average values for the clouds in the boxed region of Fig. 1. The cloud cover fraction was taken to be $A_C = 0.5$, and the altitude was taken to be $z_C = 2$ km. Radiances were then generated using a range of cloud altitudes, 1.5 km $\leq z_C \leq$ 2.5 km, surface temperatures, 289 K $\leq T_S \leq$ 295 K, and a surface reflectance at visible wavelengths for cloud-free regions, $0.01 \leq r_S \leq 0.05$. In the retrievals, the cloud altitude was assumed to be $z_C = 2.0$ km, the surface temperature was assumed to be $T_S = 292$ K, and the surface reflectance for cloud-free regions was assumed to be $r_S = 0.03$. The symbols in the figure give the assumed cloud altitude, surface temperature, and surface reflectance for cloud-free regions and the actual cloud optical depth, droplet effective radius, and fractional cloud cover used to simulate the radiances. The curves give the retrieved optical depth, droplet effective radius, and cloud cover fraction. Clearly, errors in surface temperature and cloud layer altitude have the largest effect on the retrieved cloud properties. Errors in the surface reflectance largely affect only the retrieved cloud optical depth. In the partly cloudy pixel retrieval, errors in the contribution of the cloud-free portion to the pixel radiance lead to errors in the reflectance estimated for the overcast portion and, consequently, to errors in the retrieved optical depth. The errors in cloud optical depth affect only slightly the radiative properties of the cloud at 3.7 and 11 μm and thus have little effect on the retrieved droplet effective radius and the fractional cloud cover.

The results in Fig. 12a show that, as expected, if the altitude assumed for the layer is too low, cloud cover fraction will be overestimated and, consequently, as is the case with threshold methods that assume a pixel to be overcast, when it is only partly cloud covered, cloud optical depth will be underestimated and droplet effective radius will be overestimated. The same trends occurs if the surface temperature is assumed to be too low. The opposite trends hold if cloud altitude is assumed to be too high or the surface temperature is assumed to be too high.

The ranges of errors assumed for cloud altitude, surface temperature, and surface reflectance shown in Fig. 12 are well beyond those expected for single-layered cloud systems within 50-km-scale regions. On the other hand, even with small errors in the assumed cloud altitude, surface temperature, and surface reflectance, the uncertainties in the retrieved cloud properties will be sizable when the effects of the clouds on the pixel-scale radiances are small. The effects are small when the cloud cover fraction is small, when the clouds are thin, and when the clouds are at low altitudes just above the

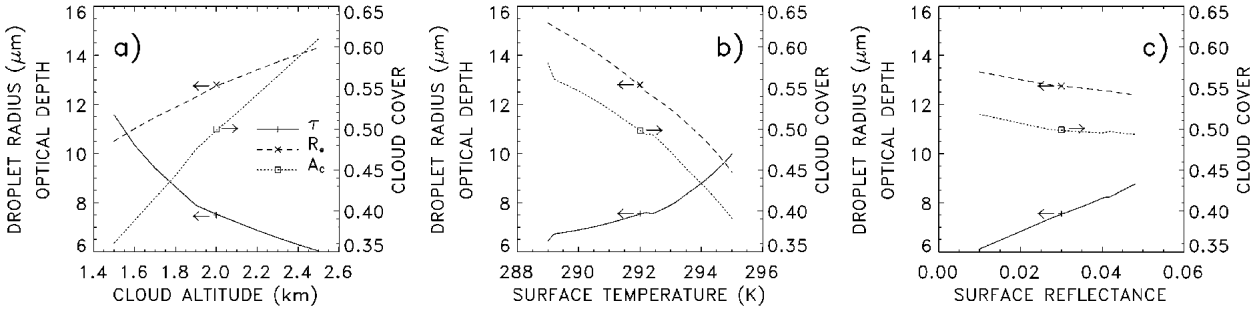

FIG. 12. Sensitivity of retrieved cloud optical depth (solid line), droplet effective radius (dashed line), and cloud cover fraction (dotted line) for partly cloudy pixels to actual values of (a) cloud altitude, (b) surface temperature, (c) and surface reflectance. The values assumed for the retrievals are $z_C = 2$ km, $T_S = 292$ K, and $r_S = 0.03$, as indicated by the symbols. The cloud properties used to generate the radiances on which the retrievals were based are optical depth, $\tau = 7.5$; droplet effective radius, $R_e = 12.8$ μm; and fractional cloud cover, $A_C = 0.5$, also indicated by the symbols. The optical depth and droplet effective radius are equal to the averages for the clouds in the boxed region of Fig. 1. The radiances and retrievals were performed for a solar zenith angle of 56°, a satellite zenith angle of 25°, and a relative azimuth angle of 100°, which are approximately equal to the averages for the boxed region in Fig. 1.

surface. Under such conditions small errors in the assumed cloud-free radiances and layer altitudes can lead to large errors in the retrieved cloud properties. An assessment of these errors was undertaken by imposing randomly selected values of the cloud-free radiances and cloud layer altitudes for a large ensemble of partly cloudy pixels. Pixels initially identified as being partly cloudy but through the retrieval process were found to be overcast or cloud-free were included in the sensitivity study. As the errors in the cloud properties are sensitive to the fractional cloud cover within the pixel and, of course, to the properties of the clouds as well, the ensemble of cases included 30 randomly selected 50-km-scale regions that contained only a single layer of low-level clouds. The ensemble members spanned a wide range of cloud conditions, from nearly overcast to nearly cloud-free, from optically thick to optically thin clouds, and from relatively high-altitude clouds ($z_C \sim 4$ km) to low-altitude clouds ($z_C \sim 0.5$ km). Uncertainties in cloud-free radiances typical of the 50-km scale were derived from large-scale cloud-free regions. For the 50-km scale, a typical standard deviation for the 0.64-μm cloud-free reflectance was 0.002 and that for the sea surface temperature was 0.4 K. Because the 3.7-μm reflectance of the cloud-free ocean is taken to be zero for the retrieval of cloud properties, the uncertainty in the reflectance was also taken to be zero. The uncertainties in cloud-free emission at 3.7 and 11 μm were calculated by allowing the sea surface temperature to vary within its range of uncertainty. Likewise, a typical value for the uncertainty in layer altitude was derived from regions that were largely overcast. At the 50-km scale a typical standard deviation in altitude for single-layered cloud systems was found to be 100 m. The cloud-free visible reflectance, sea surface temperature, and layer altitudes were represented as randomly distributed Gaussian distributions with the specified standard deviations and zero means. For each of the randomly selected 50-km-scale subregions, 400 simulations of the retrievals were performed for all pixels and the results composited.

Figure 13 summarizes the uncertainties in pixel-scale fractional cloud cover, visible optical depth, and droplet effective radius for the ensemble. The results are binned for 0.2 intervals in the pixel-scale cloud cover and represent the mean and standard deviations arising from the uncertainties in the cloud-free reflectances, sea surface temperatures, and layer altitudes. The uncertainties show small but significant biases. Cloud fraction is confined to the interval $0 \leq A_C \leq 1$. When the uncertainties in layer altitude, sea surface temperature, and 0.64-μm reflectances combine to affect the cloud fraction of pixels that are mostly cloudy ($A_C > 0.8$), the maximum value the cloud cover can take is unity. When the cloud cover is overestimated, departure of the estimated cloud cover from the actual value is small compared with the departures for cases in which the cloud cover is underestimated. The range of the cloud cover allowed in instances of underestimating cloud fraction outweigh the overestimates, and on average the cloud cover is underestimated for pixels that are mostly cloudy. The bias, however, is small, less than 0.02 in fractional cover. A similar positive bias would probably arise for the nearly cloud-free pixels, but as will be discussed in a later paper, the results obtained thus far are sparsely populated by regions that are nearly cloud-free. The sparse population stems from the avoidance of regions that lack sufficient numbers of overcast pixels to allow for a reliable estimate of cloud layer altitudes. Consequently, numerous large-scale regions with sparse cloud cover, even at the pixel scale, have not been analyzed with the current scheme. Standard deviations in the estimated cloud fractions are, of course, largest for the midranges of pixel-scale cloud fraction. At the midranges, the average departure from the existing cloud fraction reaches maximum values. Nonetheless, the pixel-scale standard deviation is typically less than 0.1.

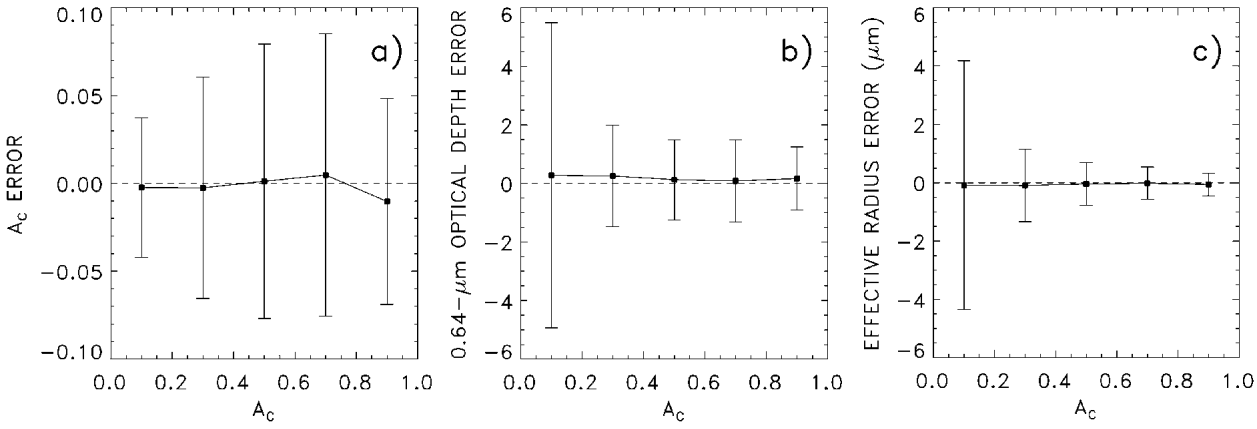

FIG. 13. Uncertainties (mean and std dev) in (a) pixel-scale cloud cover, (b) visible optical depth, (c) and droplet effective radius due to uncertainties in cloud-free 0.64-μm reflectance, sea surface temperature, and cloud layer altitudes typical of 50-km-scale regions. The uncertainties are given for 0.2 intervals in the pixel-scale fractional cloud cover.

Figure 13b shows that the optical depths retrieved for clouds that only partly cover a field of view are likewise biased. Generally, as is expected on the basis of theoretical considerations like those presented by Han et al. (1994), when the cloud cover is overestimated, the optical depth is underestimated and vice versa. The biases, however, are small, less than 0.5. Likewise, the standard deviation of the pixel-scale estimates of optical depths is acceptably small, $|\Delta\tau| < 2$, as long as the clouds in the pixel have an appreciable effect on the radiance. As cloud fraction becomes small, the uncertainty increases. For cloud cover fractions less than 0.1, the uncertainty becomes comparable to the standard deviation of the distribution of optical depths for clouds that only partially fill a field of view.

The uncertainties in the droplet effective radii retrieved for clouds that only partially cover a field of view show much the same pattern in Fig. 13c as those for the optical depths in Fig. 13b. As with the optical depths, the biases follow the expected pattern. When the optical depth is underestimated, the droplet effective radius is overestimated. For the droplet effective radii, however, the biases are essentially negligible, less than 0.1 μm. The standard deviation of the pixel-scale uncertainty in effective droplet radius is generally less than 1 μm, but as with the uncertainties in the optical depth, those in the droplet effective radius grow as the fractional cloud cover in the pixel decreases. For cloud fractions less than 0.1, the standard deviation of the uncertainties becomes comparable to the standard deviation of the distribution of droplet effective radius for clouds that only partially cover a pixel.

In summary, uncertainties in the properties retrieved for clouds that only partly cover an imager pixel are acceptably small in that pixels with detectable cloud cover, say in the range $0.2 < A_C < 0.4$, can generally be distinguished from both cloud-free pixels and from pixels in which the cloud cover ranges from $0.6 < A_C < 0.8$, which in turn can also be distinguished from pixels that are overcast.

5. Conclusions

The approach suggested by Arking and Childs (1985) has been implemented to retrieve the fractional cloud cover, visible optical depth, and droplet effective radius of clouds that only partially cover the field of view of an imager. Here the scheme is applied to 2-km imagery collected with VIRS for TRMM. The scheme is limited to single-layer cloud systems. It assumes that the clouds that only partially cover an imager pixel are at the altitude of the layer and that the layer altitude is derived from the altitudes obtained from nearby pixels that are overcast by clouds in the same layer.

A comparison of the results obtained with the partly cloudy pixel retrieval and those obtained from a typical threshold retrieval, in which all cloud-contaminated pixels are taken to be overcast, reveals the types of biases expected for threshold retrievals: cloud cover fraction and droplet effective radius are often overestimated, while cloud optical depth, cloud altitude, liquid water path, and column droplet number concentration are underestimated. Comparison of the properties of the clouds for the partly cloudy pixels with those for clouds in nearby pixels that are overcast reveals that the visible optical depths, droplet effective radii and, consequently, cloud liquid water paths are all generally smaller for the clouds in the partly cloudy pixels. Nevertheless, for pixel-scale cloud fractions $0.2 < A_C < 0.8$, the visible optical depths, droplet effective radii, and column droplet number concentrations decrease slowly with decreasing pixel-scale fractional cloud cover. Within 50-km-scale regions the properties of marine stratus and stratocumulus remain remarkably constant as the layer breaks up, with relative decreases in optical depth, droplet radius, and column number concentration on the order of 20%–30% for relative changes in cloud cover fraction of order 80%. As both optical depth and droplet effective radius decrease with decreasing cloud cover fraction, cloud liquid water path proves to be somewhat more sensitive than optical depth, droplet radius, or column droplet number concentration to pixel-scale fractional cloud cover.

The retrieved cloud properties were also investigated for their sensitivity to uncertainties in cloud-free radiances as drawn from the variability of the radiances for large cloud-free ocean scenes and uncertainties for cloud layer altitudes as drawn from the variability of altitude for large overcast scenes. Except for small pixel-scale cloud cover fractions, $A_C < 0.1$, uncertainties in the retrieved cloud properties prove to be relatively small: $|\Delta A_C| < 0.1$, $|\Delta\tau| < 2$ and $|R_e| < 2$ μm. Consequently, pixels with distinct ranges of cloud cover fraction, for example, cloud-free, $0.2 < A_C < 0.4$, $0.4 < A_C < 0.6$, $0.6 < A_C < 0.8$, and overcast, are distinguishable.

Acknowledgments. This work was supported in part by the NASA CERES Project through NAS1-98140. Part of this work was also performed while one of the authors (JAC) was a visitor in the NASA Goddard Earth Science and Technology Fellows Program at NASA's Goddard Space Flight Center. The hospitality, suggestions, and helpfulness of colleagues at Goddard were greatly appreciated. The authors also thank Mark Matheson (Oregon State University), Fu-Lung Chang (University of Maryland), and two anonymous reviewers, whose comments and suggestions greatly improved the presentation.

REFERENCES

Arking, A., and J. D. Childs, 1985: The retrieval of cloud cover parameters from multispectral satellite images. *J. Climate Appl. Meteor.,* **24,** 322–333.

Brenguier, J.-L., H. Pawlowska, L. Schüller, R. Preusker, J. Fis-

cher, and Y. Fouquart, 2000: Radiative properties of boundary layer clouds: Droplet effective radius versus number concentration. *J. Atmos. Sci.,* **57,** 803–821.

Coakley, J. A., Jr., 1987: A dynamic threshold method for obtaining cloud cover from satellite imagery data. *J. Geophys. Res.,* **92,** 3985–3990.

——, and D. G. Baldwin, 1984: Towards the objective analysis of clouds from satellite imagery data. *J. Climate Appl. Meteor.,* **23,** 1066–1099.

——, and C. D. Walsh, 2002: Limits to the aerosol indirect radiative effect derived from observations of ship tracks. *J. Atmos. Sci.,* **59,** 668–680.

——, W. R. Tahnk, A. Jayaraman, P. K. Quinn, C. Devaux, and D. Tanré, 2002: Aerosol optical depths and direct radiative forcing for INDOEX derived from AVHRR: Theory. *J. Geophys. Res.,* **107,** 8009, doi:10.1029/2000JD000182.

Han, Q., W. B. Rossow, and A. A. Lacis, 1994: Near-global survey of effective droplet radii in liquid water clouds using ISCCP data. *J. Climate,* **7,** 465–497.

Harshvardhan, S. E. Schwartz, C. M. Benkowitz, and G. Guo, 2002: Aerosol influence on cloud microphysics examined by satellite measurements and chemical transport modeling. *J. Atmos. Sci.,* **59,** 714–725.

King, M. D., and Coauthors, 2003: Cloud and aerosol properties, precipitable water, and profiles of temperature and water vapor from MODIS. *IEEE Trans. Geosci. Remote Sens.,* **41,** 442–458.

Kobayashi, T., 1993: Effects due to cloud geometry on biases in the albedo derived from radiance measurements. *J. Climate,* **6,** 120–128.

McClatchey, R. A., R. W. Fenn, J. E. Selby, F. E. Volz, and J. S. Garing, 1972: *Optical properties of the atmosphere.* 3d ed. AFCRL-72-0497, Environmental Research Paper 441, 108 pp.

Nakajima, T., and M. D. King, 1990: Determination of the optical thickness and effective particle radius of clouds from solar radiation measurements. Part I: Theory. *J. Atmos. Sci.,* **47,** 1878–1893.

——, A. Higurashi, K. Kawamoto, and J. E. Penner, 2001: A possible correlation between satellite-derived cloud and aerosol microphysical parameters. *Geophys. Res. Lett.,* **78,** 1171–1174.

Nakajima, T. Y., and T. Nakajima, 1995: Wide-area determination of cloud microphysical properties from AVHRR measurements for FIRE and ASTEX regions. *J. Atmos. Sci.,* **52,** 4043–4059.

Platnick, S., M. D. King, S. A. Ackerman, W. P. Menzel, B. A. Baum, J. C. Riedi, and R. A. Frey, 2003: The MODIS cloud products: Algorithms and examples from *Terra. IEEE Trans. Geosci. Remote Sens.,* **41,** 459–473.

Rossow, W. B., and L. C. Garder, 1993: Cloud detection using satellite measurements of infrared and visible radiances for ISCCP. *J. Climate,* **6,** 2341–2369.

——, and R. A. Schiffer, 1999: Advances in understanding clouds from ISCCP. *Bull. Amer. Meteor. Soc.,* **80,** 2261–2287.

——, C. Delo, and B. Cairns, 2002: Implications of the observed mesoscale variations of clouds for the Earth's radiation budget. *J. Climate,* **15,** 557–585.

Stevens, B., W. R. Cotton, G. Feingold, and C.-H. Moeng, 1998: Large-eddy simulations of strongly precipitating, shallow, stratocumulus-topped boundary layers. *J. Atmos. Sci.,* **55,** 3616–3638.

Szczodrak, M., P. H. Austin, and P. B. Krummel, 2001: Variability of optical depth and effective radius in marine stratocumulus clouds. *J. Atmos. Sci.,* **58,** 2912–2926.

Welch, R. M., and B. A. Wielicki, 1985: A radiative parameterization of stratocumulus cloud fields. *J. Atmos. Sci.,* **42,** 2888–2897.

Wetzel, M. A., and L. L. Stowe, 1999: Satellite-observed patterns in stratus microphysics, aerosol optical thickness, and shortwave radiative forcing. *J. Geophys. Res.,* **104,** 31 287–31 299.